1. General Introduction

This introductory section delineates a preview of the fuel cells (FCs), various types and the reactions involved, focusing mainly on oxygen reduction reaction (ORR). Recent trends in the development of Pt-free electrocatalysts over a period of time will also be discussed in this chapter. A comprehensive explanation of numerous reports on considerable attempts have concentrated on exploring Pd-based nanocatalysts with advanced stability to utilize as substitutes for Pt will also be discussed in this chapter. Especial emphasis has been given to the Pd electrocatalysts, including bimetallic and trimetallic nanoparticles (NPs) for ORR. This chapter also includes the extensive literature survey, scopes, objectives, and research plan for the present investigation.

1.1. Overview

The most vital resource for a nation's development is energy, and the amount of energy used per person is rising dramatically. Any nation's energy policy is driven by three factors: economic growth, environmental protection, and energy security, or the "three E's. The world of today is dependent particularly on fossil fuels. Fossil fuels are mainly used to generate power and heat. Since 1950, the global population has been growing, and rising living standards have resulted in a rapidly growing need for energy, which will reach its maximum in 2035, as seen in Figure 1.1a [1-9]. Furthermore, governments worldwide are considering energy security because fossil fuels like coal, oil, and natural gas are non-renewable throughout human history. Fossil fuels will eventually run out, though it might not happen in the next two decades because substantial supplies of coal and natural gas are still accessible. However, existing reserves of coal and natural gas should endure for about 200 years and 70 years, respectively, at the current pace of usage; oil is predicted to run out much sooner [3-7]. When the remaining fossil fuels run out, an alternative fuel will be required to meet the world's energy needs. This is especially true for the transportation sector, which accounts for about 60% of global energy use. The need to conserve energy and use alternative energy sources, especially renewable energy, has grown due to concerns regarding greenhouse gas emissions (Figure 1.1b), environmental degradation, and serious health problems. Therefore, new energy resources must be developed immediately to meet our energy needs more securely and sustainably. Fuel cells (FCs) and Metal-air batteries (MABs) with high efficiency and environmentally benign characteristics have attracted much attention owing to their

irreplaceable roles in the construction of the future sustainable energy system [7-13]. These technologies help lower greenhouse gas emissions, decrease pollution, and encourage sustainability for a carbon-neutral world.

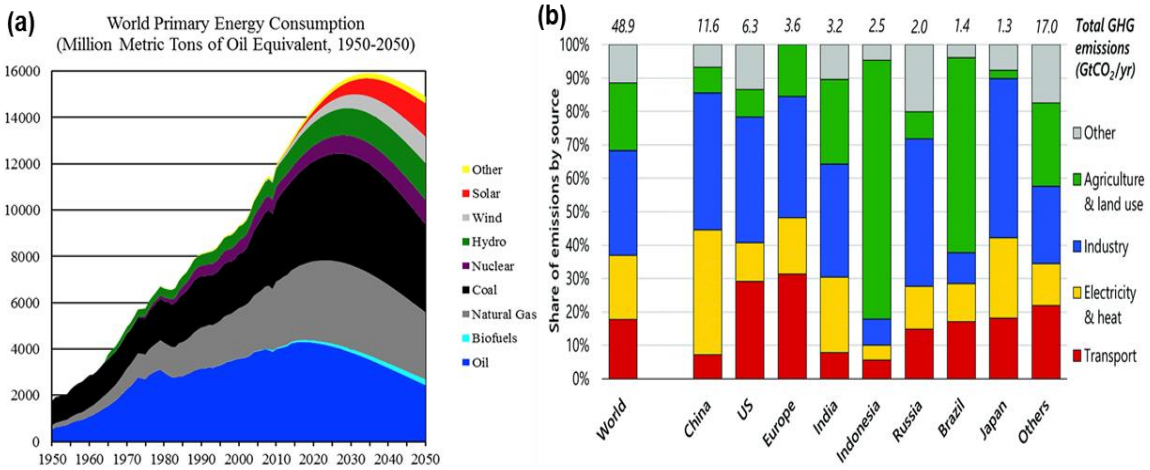

Figure 1.1: (a) World primary energy consumption (Reproduced from Reference [2]), (b) Global greenhouse gas emissions in 2014, broken down by sector and by major countries (Reproduced from Reference [3]).

1.2. Fuel Cells

FCs are electrochemical conversion devices that convert chemical energy into electrical energy without the combustion of fuels [5-9]. Instead several steps required by combustion-based heat engines, FCs directly convert chemical energy to electrical energy [11, 12]. Nevertheless, external reserves continually supply the reactants to the FC, unlike batteries, which store their reactants inside a cell. FCs are considered one of the most potential technologies that have significantly impacted renewable energy advancement. The first FC was established over a century ago and is currently the subject of further research as the world strives to become carbon-neutral. In addition to its great energy efficiency and minimal emissions, FCs have several other benefits, including a high energy density, compact design, and conspicuous performance. Since FCs only produce water as a byproduct and don't require conventional fuels like petrol or oil, they can reduce economic reliance on nations with unstable political systems. On the other hand, the FCs fuels may be produced everywhere and at varying scalable volumes, eventually resulting in a more decentralized and stable power system. When operating on

clean, renewable resources, FC systems can achieve nearly zero CO_2 emissions and are the most efficient compared to traditional energy systems. FCs are primarily composed of two porous electrodes, one of which is positively charged, known as the cathode and the other negatively charged, known as the anode. Both are in contact with an electrolyte layer. The catalysts on both electrodes accelerate the electrochemical reactions and an electric current is generated by the electrochemical processes [9-17].

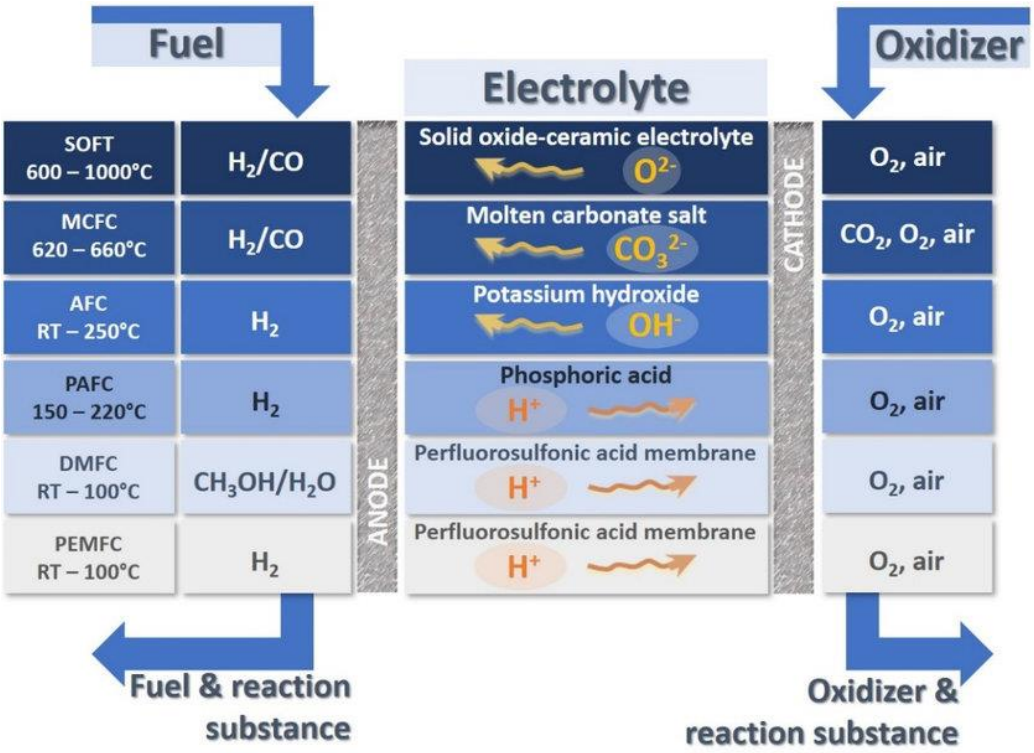

Figure 1.2: Overview of the various types of FCs with their operation temperatures. (Reproduced from Reference [13]).

FCs are classified mainly on the types of fuels and electrolytes employed. Based on this, they are classified into the following types [15-23]: (1) phosphoric acid FCs (PAFCs) with an acidic electrolyte solution (e.g. phosphoric acid), In PAFC, H_3PO_4 is used as an electrolyte and carbon paper as an electrode. The H^+ ion acts as a charge carrier in this type of FCs. Across the electrolyte, these ions move from the anode to the cathode and the released electrons return to the cathode via the external circuit to provide electricity. (2) Alkaline FCs (AFCs) with alkaline electrolyte solution (e.g. KOH). The AFC produces electricity using KOH in an aqueous solution. Electrical energy can be acquired and a circuit may be formed thanks to the OH^- moving across the electrolyte. (3)

Molten carbonate FCs (MCFCs) with molten carbonate salt electrolyte. They are the high temperatures FCs. They employ a molten salt mixture of carbonate immersed in a porous ceramic matrix of solid beta-alumina electrolyte that is chemically inert. (4) Proton exchange membrane FCs (PEMFCs), also known as polymer electrolyte membrane FCs with proton exchange membrane. PEMFCs are lighter and more compact than other FCs while providing a high power density. These FCs employ carbon supported platinum (Pt) or Pt alloy catalyst as electrodes and a solid polymer as the electrolyte. (5) Direct methanol FCs (DMFCs) with methanol as fuel. In DMFCs, methanol is employed as a fuel. They do not have many fuel storage challenges common to various FC systems since methanol has a greater energy density than hydrogen but a lower energy density than other fuels (petrol or diesel). Due to its liquid nature, similar to gasoline, methanol is more easily transported and supplied to the common people utilizing our current infrastructure. (6) Solid oxide FCs (SOFCs) with ceramic ion conducting electrolyte in solid oxide form. The SOFCs are also high-temperature FCs that run on solid electrolytes (solid ceramic of metallic oxide). Moreover, a range of fuels, including hydrogen, hydrocarbons, carbon monoxide, etc., can be used in SOFC. Figure 1.2 represents the operation of different types of FCs. Applications for various types of FCs are frequently very different from one another [15-23].

Among various FCs, PEMFCs gained increasing demand due to their high power density, low temperature maintenance, good thermal/chemical stability, quick start-up, simple structure, and high energy conversion efficiency. PEMFCs are excellent choices as the primary power source for vehicles and buses. FC vehicles, or FCVs, have significant benefits against electric vehicles (EVs) powered by batteries and are considered one of the most excellent alternatives for the automobile sector [19-21]. The Toyota Mirai, which means "future" in Japanese, is the first-ever mass-made FCV. It has been marketed commercially in Japan since 2014 and is highly expensive (around $51,000 US dollars). The substantial Pt content in Mirai's FC stacks significantly contributes to its expensive market price. At the anodic part of PEMFC, hydrogen undergoes oxidation known as hydrogen oxidation reaction (HOR) to produce protons (H^+) and electrons (e^-s) ($H_2 \rightarrow 2H^+ + 2e^-$), which are transported to the cathode via the PEM and an external circuit, respectively. At the cathodic part, the incoming H^+ and e^- reduced oxygen to produce water ($1/2O_2 + 2H^+ + 2e^- \rightarrow H_2O$) known as the oxygen reduction reaction (ORR). Highly dispersed carbon supported Pt-based NPs are used to accelerate the rate of HOR

and ORR. The HOR kinetics is more rapid than the cathodic kinetics of ORR. As a result, a higher amount of Pt loading (~0.4 mg cm^{-2}) is required in ORR than in the HOR (0.05 mg cm^{-2}) to obtain the desired FC performance. As seen in Figure 1.3, Pt is a precious and less abundant metal. It would, therefore, be beneficial to lessen its loading or possibly replace it entirely with a readily available, low-cost metal. Therefore, much research is going on to design cost-effective catalysts for ORR [12, 19-28].

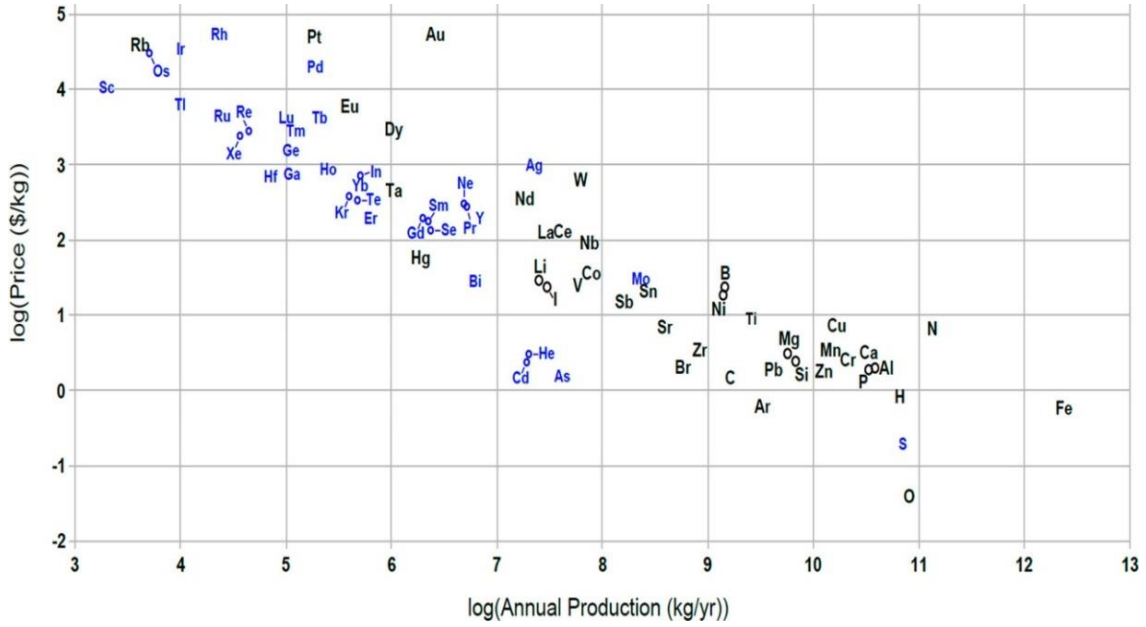

Figure 1.3: Price of the elements (in $/kg) versus their annual production (in kg/yr) (Reproduced from Reference [31]).

1.3. Oxygen Reduction Reaction

As mentioned earlier, it is the most significant reaction in chemical and biological energy conversion systems. The electrochemical ORR process has gained popularity because it typically occurs at the cathode region of different FCs, where oxygen is reduced electrochemically. Oxygen electrochemical reduction is dependent on its molecular structure. The bond order and energy of the O_2 molecule are 2 and –498.7 kJ mol^{-1}, respectively. The breaking of the O═O bond is fundamental for the electrochemical reduction process. It is widely accepted that superoxide ion (O^{2-}) formation is a critical step in ORR even though the bond energy of O^{2-} is –350 kJ mol^{-1}. The ORR process comprises a range of simultaneous continuous reactions integrated with

a few basic steps. This reaction occurs in both alkaline and acidic electrolytes and the electrolyte has a major influence on the reaction potential. Determining the reaction mechanism is challenging due to the formation of different intermediate products. It can be broadly classified into two categories [28-37]:

Alkaline medium: (1) Direct $4e^-$ pathway: O_2 molecule is directly reduced to the OH^-. The reaction pathway can be written as:

$$O_2 + 2H_2O + 4e^- \rightarrow 4OH^- \qquad E^\circ = +0.401 \text{ V } \textit{vs.} \text{ SHE}$$

(2) Indirect two-electron reaction pathway: O_2 molecule is partially reduced, HO_2^- as intermediate and then to OH^-. The reaction pathway can be written as:

$$O_2 + H_2O + 2e^- \rightarrow HO_2^- + OH^- \qquad E^\circ = -0.076 \text{ V } \textit{vs.} \text{ SHE}$$

$$HO_2^- + H_2O + 2e^- \rightarrow 3OH^- \qquad E^\circ = +0.878 \text{ V } \textit{vs.} \text{ SHE}$$

or decomposition: $2HO_2^- \rightarrow 2OH^- + O_2$

Acidic medium: (1) Direct four-electron reaction pathway: O_2 molecule is directly reduced to the H_2O. The reaction pathway can be written as:

$$O_2 + 4H^+ + 4e^- \rightarrow 2H_2O \qquad E^\circ = +1.229 \text{ V } \textit{vs.} \text{ SHE}$$

(2) Indirect two-electron reaction pathway: oxygen molecule is partially reduced, HO_2^- as intermediate and then to OH^-. The reaction pathway can be written as:

$$O_2 + 2H^+ + 2e^- \rightarrow H_2O_2 \qquad E^\circ = +0.695 \text{ V } \textit{vs.} \text{ SHE}$$

$$H_2O_2 + 2H^+ + 2e^- \rightarrow 2H_2O \qquad E^\circ = +1.776 \text{ V } \textit{vs.} \text{ SHE}$$

or decomposition: $2\,H_2O_2 \rightarrow 2H_2O + O_2$

The direct or full reduction pathway is more effective which follows the $4e^-$ pathway and required low overpotential (Figure 1.4a). The other process can occur via an indirect or partial reduction pathway, using a $2e^-$ route to produce adsorbed H_2O_2 (Figure 1.4b). The former is the preferred approach when selecting a catalyst for the ORR due to its increased efficiency and the unstable nature of H_2O_2 compared to the stable nature of H_2O [26-38]. For the indirect pathway to occur, O_2 must first be adsorbed onto the surface of the catalyst. Thereafter, two H^+ additions take place, generating an adsorbed H_2O_2. The resultant H_2O_2 molecule can then go through more reduction to provide two H_2O molecules or dissociate, yielding a free H_2O_2. The direct reduction pathway is a dissociative adsorption process that starts with the O_2 adsorption on the surface of the catalyst. After the adsorption of O_2, the first e^- transfer occurs with the addition of H^+,

producing *OOH. The second e^- transfer happens, this time in the form of another addition of hydrogen. The progress of the reaction depends on whether the second H^+ addition occurs at the O_2 molecule adsorbed to the electrocatalyst or at the oxygen that was previously attached to the H^+.

Table 1.1: ORR mechanisms on the catalyst surface [33, 35]

Mechanism 1	Mechanism 2
$O_2 \rightarrow *O_2$	$O_2 \rightarrow *O_2$
$*O_2 + e^- + H^+ \rightarrow *OOH$	$*O_2 + e^- + H^+ \rightarrow *OOH$
$*OOH + e^- + H^+ \rightarrow *OH + *OH$	$*OOH + e^- + H^+ \rightarrow *O + H_2O$
$2*OH + 2\,e^- + 2H^+ \rightarrow 2H_2O + *$	$*O + e^- + H^+ \rightarrow *OH$
	$*OH + e^- + H^+ \rightarrow H_2O + *$

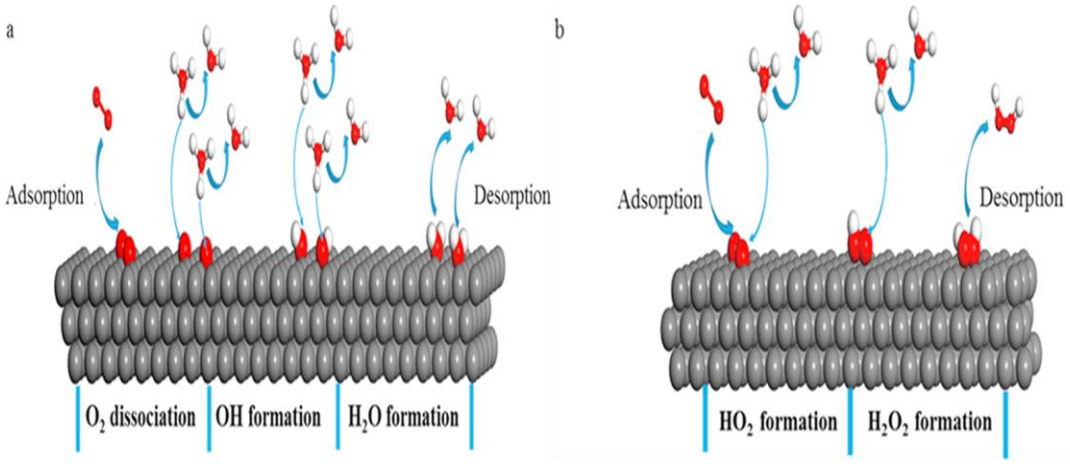

Figure 1.4: Proposed mechanism schematics of (a) full reduction and (b) partial reduction of oxygen (Reproduced from Reference [38]).

The electrocatalyst will have two adsorbed OH groups in case the second H^+ addition occurs at the adsorbed oxygen to the electrocatalyst (mechanism 1, Table 1.1). At each *OH group, successive e^- transfers take place in the form of the addition of hydrogen, producing two molecules of H_2O molecules and O atoms that have been adsorbed desorb in case the second H^+ addition occurs at the oxygen that was previously attached to the first H^+ (mechanism 2, Table 1.1). An H_2O water molecule desorbs after two subsequent transfers of e^- in the form of H^+ addition to the *O. According to Density

functional theory (DFT) simulations of the two paths, the more plausible approach is mechanism 1, which is thermodynamically preferred [26-38].

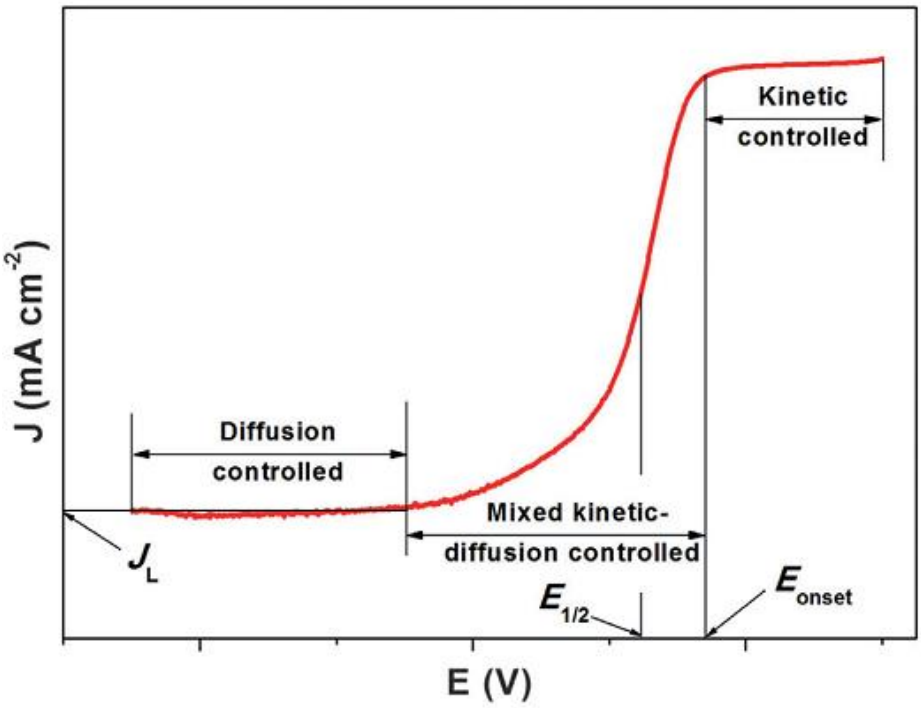

Figure 1.5: Typical ORR polarization curve (Reproduced from Reference [28]).

The ORR polarisation curves are typically used to evaluate the electrocatalyst data. These curves normally show three regions throughout the potential range: the diffusion limiting region, the kinetic control region, and the kinetic-diffusion mixed control region (Figure 1.5) [25, 32]. The speed of ORR is sluggish in the kinetically controlled region and the current density gradually rises as the potential drops. In the mixed kinetic-diffusion controlled region, the current density increases noticeably as the reaction speeds up and the potential decreases. The current density in the diffusion-controlled zone rotates at a specific rate to reach a plateau region, depending on the rate at which reactants diffuse. Two metrics are typically used to qualitatively confirm the activities of catalysts: onset potential (E_{onset}) and half-wave potential ($E_{1/2}$). A higher potential value indicates higher activity of the catalyst towards ORR. On the other hand, different publications define the E_{onset} in various ways. According to some definitions, the E_{onset} can be defined as a potential equal to 5% of the diffusion-limited current density (J_L). The potential where the reaction begins is known as E_{onset} and is often determined as the potential where the slope of CV reaches beyond the threshold value of current density (0.1 mA

cm^{-2}). An additional fundamental parameter, $E_{1/2}$, is obtained from the middle point of the LSV plot at 1600 rpm. This potential is equal to half of the limiting current density ($j_{L)}$. The current density that is limited by the rate at which ions diffuse to the electrode surface is known as the j_L and it is controlled by mass transport. The applied voltage no longer affects the current in this range [25, 32, 36-39].

The kinetic current density (jk), irrespective of the mass transfer limitations, can be calculated using the following Koutecky–Levich (K–L) equation [28]

$$1/j = 1/j_L + 1/j_K = 1/B\omega^{1/2} + 1/j_k \quad (1)$$

where, $B = 0.629nFC_o(D_o)^{2/3}\nu^{-1/6}$

$j_K = nFkC_o$

where, j = current density, j_k= kinetic current density, j_l= diffusion limited current density, B = slope of the K−L plot, ω = rotating rate of the RDE (rad/s), n = number of e^- transfer per O_2 molecule, F = Faraday constant (96485 C mol^{-1}), D_{O2} = diffusion coefficient of O_2 (1.9×10^{-5} cm^{-2} s^{-1}), v = kinematic viscosity (0.01 cm^{-2} s^{-1}) and C_{O2} = bulk concentration of O_2 (1.1×10^{-6} mol cm^3) in 0.1M KOH and k = electron transfer rate constant.

A plot of j^{-1} vs. $\omega^{-1/2}$ should be linear and j_K and n can be calculated from the intercept and slope, respectively. A value of n = 2 and 4 decides the e^- pathway of ORR.

1.3.1. Need of electrocatalyst for ORR

It is well understood that the ORR plays a vital role in numerous energy conversion devices. Still, the intrinsically sluggish nature due to the huge overpotential of ORR limits the overall efficiency of energy-conversion devices. Therefore, an appropriate electrocatalyst is required that can effectively influence the kinetics of reactions and direct ORR toward more efficient pathways. As a result, developing novel cathode electrocatalysts has recently become a key focus of industrial and academic research [36-48]. As per the DFT calculations, ORR catalytic performance correlates with the binding energy (BE) between oxygenated species and the surface of the catalyst. According to the Sabatier principle, a reactant should bind to a catalyst both firmly enough to cause a reaction to occur and weakly sufficient to cause the product to dissociate and prevent either the reactant or any intermediates from poisoning the catalyst surface. Therefore, in this instance, the oxygen intermediate should be firmly bound to the electrocatalyst

enough for the reaction to occur on the interface but not too strongly that oxygenated species contaminate the electrocatalyst. It is possible to develop "volcano plots" like the one shown in Figure 1.6, correlating catalytic activity to the BE of oxygen species using experimental data and numerical simulations. To determine the ideal BE for ORR electrocatalysts, these plots can then be analyzed. Pt catalysts hold the ideal position among the catalysts considered in Figure 1.6; however, it is not at the volcano's highest position [36, 47].

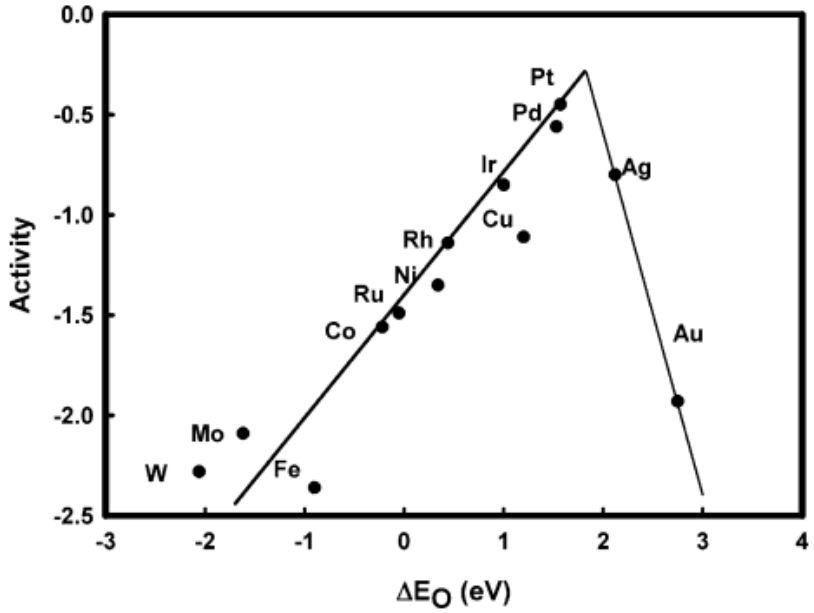

Figure 1.6: Trends in oxygen reduction activity (defined in the text) plotted as a function of the oxygen binding energy (Reproduced from Reference [48]).

As a result, the construction of an ORR electrocatalyst still has space for development. One way to alter the adsorption energies of oxygen intermediates is to modify the catalyst's conductive band or *d*-band center. The adsorption energies have been demonstrated to correspond with the *d*-band, which represents the electronic properties of the solid. It has been found that the *d*-band center correlates with adsorption energies and serves as a descriptor of the solid's electronic characteristics [36, 47]. It has been observed that in bimetallic electrocatalysts, tuning the morphology and predominant facets can change the *d*-band center's position in relation to bulk metals.

Pt stands out as the ideal catalyst among present pure metals because it possesses all the necessary properties for an effective ORR. The slow ORR kinetics, however, require a more significant loading of the Pt catalyst. Since Pt is a noble metal in and of

itself, the limited supply of Pt, CO poisoning, durability concerns, poor tolerance to methanol in DMFCs and its high price emerge as further obstacles. Overall, the limitations above prevent the widespread practical use of FCs, even though alkaline FCs using Pt as an ORR catalyst have been successfully constructed for the Gemini and Apollo spacecraft flown by NASA in the 1960s. Although efforts to lower the Pt catalyst content have been made recently, it has been observed that Pt can readily migrate and agglomerate over the carbon support when employed as a cathodic candidate. Furthermore, smaller Pt NPs dissolve in solution and produce Pt cations that can subsequently deposit upon other Pt NPs and induce them to accumulate and deactivate. This process results in the usage of a significant amount of Pt. Thus, efforts have also been focused on developing substitutes, including alternative noble metals with comparatively inexpensive materials, non-noble metals, and metal-free catalysts [36, 45, 48].

1.3.2. Pd-based electrocatalysts

Pd-based materials have garnered significant interest as substitute electrocatalysts due to their similar characteristics and marginally lower price than Pt. In the past decade, from 2010 to 2020, the average costs of Pd and Pt per troy oz are $910.62 and $1230.96, respectively [43]. In particular, Pd and Pt have comparable chemical properties because they belong to the same group of Pt and are positioned next to each other in the periodic table. Pd and Pt have many similar physical and chemical characteristics. It was reported that Pd-based catalysts were more resistant to CO poisoning, highly stable in acidic environments, and more tolerant to methanol than Pt-based catalysts [43, 44]. In contrast to Pt/C, Pd-based electrocatalysts do not exhibit a methanol oxidation peak over 0.7 V on Pt/C, leading to a negative shift in the net cathode current and a notable rise in overpotential. Therefore, in methanol, Pd-based electrocatalysts show superior selectivity towards ORR compared to Pt-based catalysts. Because of its inherent characteristics, a pure Pd catalyst finds it challenging to obtain Pt-like stability and activity towards ORR. The strong affinity of Pd for oxygen prevents oxygen from being reduced. So, the ORR performance of Pd-based catalysts can be significantly increased and the price of the electrocatalysts further decreased by combining with other elements, particularly transition metals [43, 49-53].

1.3.2.1. Pd-based bimetallic electrocatalysts

Pd-based electrocatalysts have received a lot of interest owing to their analogous physical structures, including the *fcc* crystal structure and a similar atomic radius, comparable performance and lower price than Pt. Extensive research has shown that pure Pd and Pd-based electrocatalysts have higher catalytic activity and stability than Pt-based ones. Furthermore, it was demonstrated that Pd-based electrocatalysts had significantly greater methanol tolerance and resistance to CO compared to Pt-based electrocatalysts [43, 44, 47]. Therefore, it is highly desirable and necessary to create high-efficiency and cost-effective Pd-based catalysts to significantly improve ORR performance. While ORR catalysts are projected to have the qualities of low cost, high activity, and high stability synchronously, they still do not meet all the requirements for implementing FCs. To achieve this, several techniques have been developed for further enhancing the ORR performance of Pd-based electrocatalysts with fine control over the shape, composition, crystal plane, and surface strain while observably reducing the Pd usage and modifying the electronic structure [43, 44, 48-53].

Numerous Pd-based alloy NPs with different compositions have been explored in recent years. As a result, increased ORR performances of these alloy systems have been observed. We synthesized the PdNi alloy system and studied its ORR performance. As-prepared Pd_3Ni/C NPs are superior to the commercial Pt/C and Pd/C electrocatalysts. The increased performance of Pd_3Ni/C is primarily due to the downward shift of *d*-band center of Pd, larger ECSA, and uniform distribution of the PdNi NPs on the carbon matrix. The computational analyses also demonstrated the downward shift of *d*-band center of Pd for Pd_3Ni/C, which makes it superior to all other electrocatalysts [50]. Jaramillo and co-workers reported the electron-beam PVD synthesis method to synthesize $Ag_{1-x}Pd_x$ thin films with $0 \leq x \leq 1$. The designed nanomaterials and nanofilms remained constant after electrochemical measurements, inferred from XRD and XPS analysis. Based on experimental findings and DFT simulations, the observed ORR activity improvements are mainly ascribed to electronically increased Pd active sites by introducing Ag atoms within the lattice via ligand or strain factors that result in enhanced oxygen BE [51]. In another study, Zhang *et al.* found that PdCo encapsulated in N-doped porous carbon (PdCo@NPNC) synthesis and studied their catalytic behaviour toward

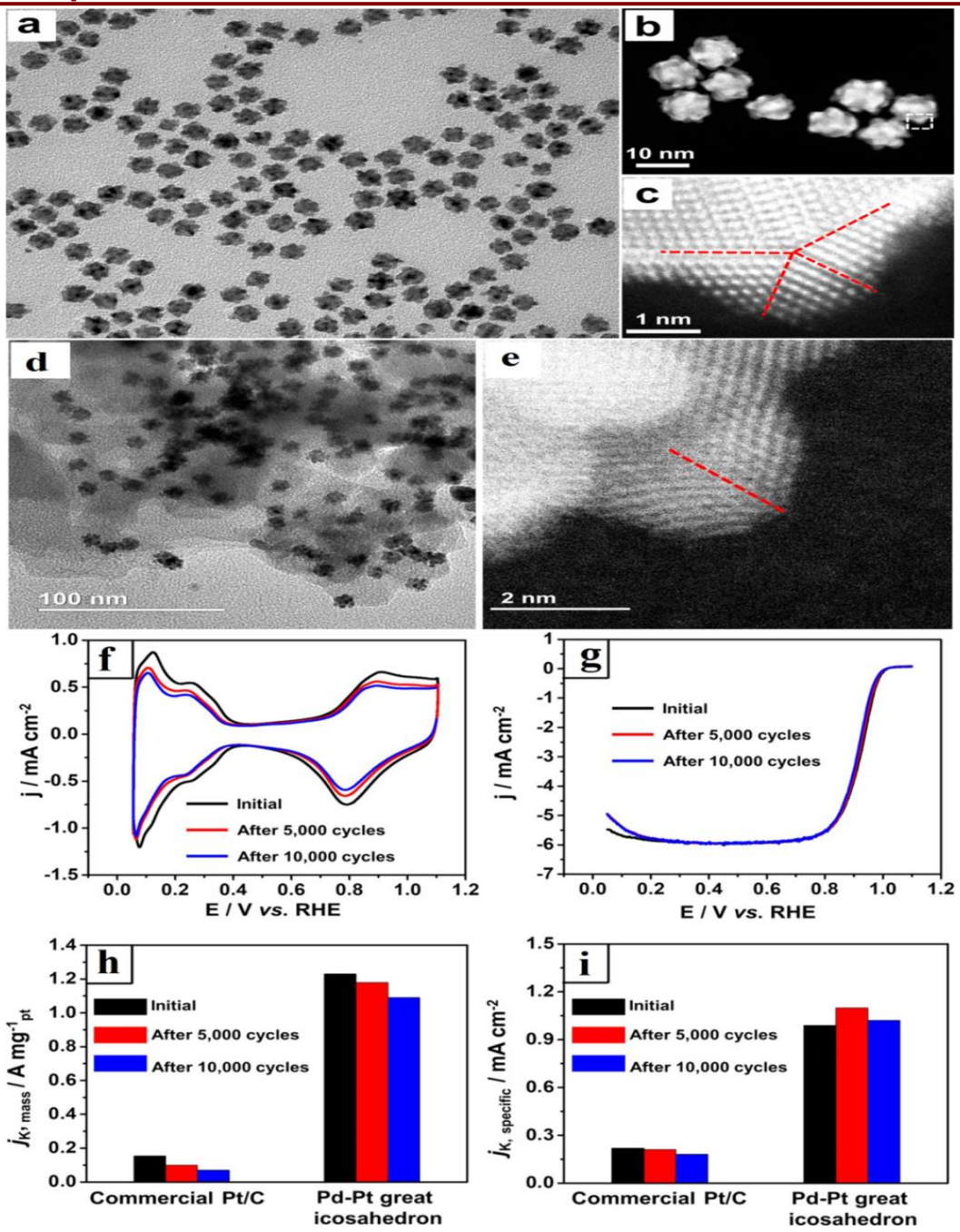

Figure 1.7: (a) TEM and (b) HAADF-STEM images of the as-obtained Pd−Pt great icosahedra, (c) atomic-resolution STEM image taken from the corner region of a great icosahedron, as marked by the box in panel (b), the twin boundaries are labelled with red dashed lines, (d) TEM and (e) HAADF-STEM images of the carbon-supported Pd−Pt great icosahedra after 10000 cycles of ADT, Benchmarking of the Pd−Pt great icosahedra against the commercial Pt/C catalyst (f) CV and (g) oxygen reduction polarization curves recorded from the Pd−Pt great icosahedra before and after 5000 and 10000 cycles of

ADT, (h) mass activities (MA) and (i) specific activities (SA) of the catalysts at 0.9 V *vs* RHE before and after ADT (Reproduced from Reference [55]).

ORR. The carbon shell prevents the NPs from coagulation, detachment and dissolution while the FC operates. The optimized PdCo@NPNCs outperform the benchmark Pt/C and Pd/C catalysts in electrocatalytic performance and enhanced durability for ORR, owing to their unique structures and chemical compositions [52]. Significant advancements have been made in recent years in preparation techniques for various morphology-controlled NPs. These size and shape-controlled NPs replicate the catalytic activity of bulk metal, while they exhibit more catalytic activity because there are more active sites. To this end, Wang *et al.*, Pd nanobelts (NB) catalysts with expanded lattice were designed by a simple solvothermal method. It was found that as-synthesized Pd-nanobelts possess extended lattices that shift the *d*-band center positively. The interaction of oxygen 2p states with the metal d states may be enhanced by an upshifting in the *d*-band center. The additional adsorbate onto the Pd-surface is also altered by a change in the d-center, which improves the catalytic activity and durability [53]. Similarly, Li and coworkers synthesized the highly wrinkled Pd nanosheets (HW-PdNs). Compared to standard Pd nanosheets (PdNs), benchmark Pd/C, and Pt/C, the HW-PdNs showed significantly increased catalytic performance. The high catalytic performance of the electrocatalysts is primarily attributed to the compressive strain created from the wrinkle structure that reduces the binding strength of adsorbed oxygen-intermediate and results in rapid kinetics toward ORR [54].

It was reported that Pt nucleation and growth were confined to the vertex of Pd icosahedral seeds, resulting in Pd–Pt icosahedra with multiple twinned Pt dots. Twin defects can also boost the ORR performance of Pt NCs by utilizing the surface strains generated by the defects. Figure 1.7 (a-c) represents the TEM and HAADF-STEM images of the Pd−Pt icosahedra. The ORR activity and durability of the Pt dots are much higher than the commercial Pt/C because of their highly twinned shape and robust anchoring to the Pd surface. An ADT was also used to investigate and compare the stability of the Pd–Pt icosahedra to that of Pt/C. CV and LSV plots were plotted after 5000 and 10000 ADT cycles. TEM and HAADF-STEM characterization of the Pd−Pt icosahedra was done after the ADT operation to understand the durability improvement (Figures 1.7d and e). A minimal change in peak potential and J_k was observed, as presented in Figure 1.7f and g,

respectively. After 10,000 redox cycles, a rise in the MA (Figure 1.7h) and SA (Figure 1.7i) of the Pd–Pt icosahedra was observed compared to the commercial Pt/C. On the carbon support, the catalytic NPs were still evenly distributed and barely agglomerated or detached. The improved stability of as-synthesized catalysts was facilitated by their high specific surface area and concave structure, which allowed for additional anchoring sites on the carbon support [55].

1.3.2.2. Pd-based trimetallic electrocatalysts

Numerous investigations have demonstrated that adding a second element to Pd can change its electronic arrangement, increasing electrocatalytic activity. Furthermore, introducing a third component into a binary system increases active sites and interactions among the three metals, increases electron density at the active sites, and reduce Pd loading [56-58]. For instance, Wang *et al.* reported the synthesis of nanothorn PdCuAu electrocatalysts displayed enhanced ORR activity, stability, and excellent tolerance to methanol [59]. In another work, PdPtCo ternary nanorings were developed via a facile template-directed process. With the maximum edge to surface ratio and ternary structure, the $Pd_{55}Pt_{18}Co_{27}$ exhibits enhanced ORR electrocatalytic activity, delivering a lower Tafel slope and the largest electrochemically active surface area (ECSA) [60]. In the same way, PtPdCu [61] was fabricated by a one-step synthetic approach. The PtPdCu displays improved ORR activity with more positive $E_{1/2}$ and E_{onset} of 0.94 and 1.0V *vs*. RHE higher than the most reported electrocatalyst. Kong *et al.* reported the synthesis of Pt–Pd–Ni octahedral nanocages. The synthesized nanomaterial exhibited the highest MA (1.17 A/mg_{Pt}) and SA (3.8 mA/cm^2). The remarkable activity and stability of the Pt–Pd–Ni octahedral nanocages are explained by the high vacancy formation and compressive strain effect [62]. Du and coworkers reported the synthesis of $Pd_{0.75}Pt_{0.25}Fe/C$ by varying the elemental proportion of Pd and Pt. $Pd_{0.75}Pt_{0.25}Fe/C$ displays the highest intrinsic activity thanks to the ligand and lattice strain effect. The adsorption energy of the oxygen intermediate is substantially decreased by the strain effect, facilitating the $Pd_{0.75}Pt_{0.25}Fe/C$ to improve the ORR activity [63]. In 2020, Wang and coworkers designed staggered PdAuRu nanothorns using KBr and DM-970 as structure-directing agents and surfactants, respectively, via a wet-chemical reduction process [64]. The nanothorns were with an average length of around 200 nm. The PdAuRu show a high SA (2.99 $mAcm^{-2}$) and MA of (1.376 $mA\mu gPd^{-1}$), respectively, better than the commercial Pt/C and Pd black for

ORR in 0.1M KOH, Additionally, an ADT shows that PdAuRu NSAs are more durable than Pt/C. The nanothorn structure and trimetallic composition, which result in more active sites and a lower Pd-O band energy, are attributable to better activity and stability Pt/C. In another report, $Mo_{0.2}Pd_3Ni$/NC exhibited $E_{1/2}$ of 0.90 V and MA of 0.78 Amg_{Pd}^{-1}, double the Pt/C (0.38 Amg_{Pt}^{-1}) toward ORR. $Mo_{0.2}Pd_3Ni$/NC has excellent stability, losing only 15% of the initial current density after 36,000 seconds. DFT and micro-structured analyses demonstrated that the *d*-band center of Pd was downshifted by the synergistic effect between Ni and Mo. This, in turn, decreased the intermediates' binding energy with Pd, decreasing the threshold energy towards ORR [65]. Sheng and coworkers have observed that $Co_{0.2}Sn_{0.2}Pd_{0.2}$/rGO shows superior ORR performances and stability among $Co_{0.2}Sn_xPd_y$/rGO (x + y = 0.4) catalysts. These catalysts were successfully prepared using reduced graphene through an ultrasonic irradiation process. The $Co_{0.2}Sn_{0.2}Pd_{0.2}$/rGO displays the $E_{1/2}$ of 0.91 V and the Tafel slope of 57 $mVdec^{-1}$. XPS results show the BE of metallic Pd shifts to a higher BE in the reported catalysts, suggesting that Pd electronic centre shifts while alloying with Co and Sn. The $Co_{0.2}Sn_{0.2}Pd_{0.2}$/rGO was continuously stable for 36,000 seconds while retaining 85.31% of the initial current density demonstrating its excellent stability even at a very low Pd content [66]. Li *et al.* constructed PdCuCo nanoalloys with varying compositions. Among these compositions, the $Pd_{59}Cu_{30}Co_{11}$ contains abundant defects and exhibits superior durability for the $Pd_{59}Cu_{30}Co_{11}$ ORR. The catalyst also exhibits a better tolerance to methanol/ethanol than the state-of-the-art Pt/C catalyst. The superior activity of the dendritic $Pd_{59}Cu_{30}Co_{11}$ nanoalloys is ascribed to a combination of effects such as defects, synergistic interaction, change in the Pd *d*-band center, and surface strain [67]. Gao and coworkers adopted a facile chemical reduction approach to synthesize nitrogen-doped graphene-supported PdNiM (M = Cu or Sn) alloys. The PdNiM (M = Cu or Sn) nanocatalysts were investigated for ORR in an alkaline medium and characterized using various physicochemical techniques. The characterization results show well-dispersed PdNiM (M = Cu or Sn) NPs over graphene support and are highly alloyed. PdNiM (M = Cu or Sn) shows excellent ORR performance and electrostability, outperforming benchmark Pt/C and Pd-black. These findings suggest that including Sn or Cu as a third element in a PdNi-based catalyst significantly increases its catalytic efficiency while lowering the Pd content [68].

1.3.2.3. Pd-MOx electrocatalysts

Transition metal oxides have garnered significant interest as very efficient ORR electrocatalysts. TMOs are able to combine with other materials, durability against alkaline corrosion, availability, affordability, and changing oxidation state all contribute to improved ORR performance. Additionally, the aggregation of the metal NPs is inhibited by the crystalline structure of transition MOs. Prior to being used as electrocatalysts; TMOs must first enhance their conductivities because the majority of them are semiconductors. Although several methods have been employed, noble metal-based TMO catalysts are thought to be effective in improving the performance of noble metal catalysts and TMO's interparticle conductivity [69-71]. When noble metals and TMO catalysts are combined, they have a more significant synergistic effect on ORR than when used alone [70]. Through the redox process of TMOs, they function as an oxygen reservoir. This oxygen reservoir increased ORR activity by promoting oxygen diffusion to noble metal catalysts (Pd/Pt). In addition, oxygen supply to the catalytically active sites of noble metals has also boosted the electronic interaction between the metal and metal oxide, resulting in increased activity [72-74]. Woo and coworkers reported that Pd–Mn_3O_4 was developed by polyol reduction and thermal decomposition methods. Mn_3O_4 facilitates the transport of oxygen to Pd's active sites, improving activity towards ORR. The ADT reveals Pd–Mn_3O_4 catalyst displays the highest durability, 149% in MA and 142% in SA, than the Pd/C. The strong interaction between metal (Pd)-metal oxide (Mn_3O_4) enables the redox of Mn_3O_4 to facilitate transport of oxygen to the active sites of Pd, is attributed to the higher performance [73]. Zhang *et al.* reported the synthesis of Pd–WO_3/C and explored the activity towards ORR. They observed a slight shift of BE in the XPS spectrum of Pd–WO_3/C than the Pd, which was ascribed to the electron modification due to WO_3. This electron modification also results from the interaction between Pd and WO_3, and as a result, it improves the ORR activity [74]. In another work, Sahoo and coworkers have developed a Pd-Fe_2O_3/NGO-CNT nanohybrid. Pd/Fe_2O_3 NPs are uniformly distributed over the NRGO-CNT proved via different characterization techniques. The UV-Vis and FT-IR spectra indicate abundant defects and oxygenated functional groups on the surfaces of GO and NRGO. These factors contributed to the Pd-Fe_2O_3/NRGO-CNT nanohybrid's superior electrochemical performance compared to the Pd/NRGO, Pd/NRGO, and benchmark Pt/C catalysts [75].

1.3.3. Role of carbon support

Carbon-support nanomaterials include carbon black (CB) (*e.g.* Vulcan, Ketjen), carbon nanotubes (CNTs), graphene and carbon nanofibers (CNFs) are the most widely used support materials for catalysts' NPs towards ORR [76-82]. The unique electrical, mechanical, and huge specific surface area features of carbon have drawn much interest in it as a promising catalyst support. These support materials improve the mass transfer effect of the reactant to the catalysts and enhance the catalysts surface area for the transfer of electrons. The interactions within the metal NPs and carbon support results in strong metal–support interactions, which increases ORR activity. These materials also increase the stability of metal NPs by preventing them from Ostwald ripening, sintering, or agglomeration and dissolution. Due to their abundant accessibility, excellent conductivity, and affordable cost, carbon blacks, particularly Vulcan XC-72R, are the most often utilized carbon materials for noble metal based catalysts. Moreover, graphene is a planar sheet of two-dimensional sp^2-carbon atoms arranged hexagonally [76-79]. Its remarkable physical and chemical characteristics, such as fast charge transfer, incredible electrical and thermal conductivities, superb mechanical flexibility, amazing elasticity, and large surface area, have gained significant attention. As a result, researchers are now investigating graphene and graphene-based materials as potential catalyst supports for PEMFCs [80-82].

1.4. Objectives of the Present Work

Motivated by the groundbreaking discoveries of the reported works in the literature described in the preceding sections, we have formulated the subsequent goals, which are briefly stated below:

1. To synthesize carbon supported trimetallic and bimetallic NPs of type PdM^1M^2 (M^1/M^2 = Cu, Fe, Ag, Co) in various compositions via the typical solvothermal method.
2. To synthesize ultralow Pd content on CuO_X/C via the typical solvothermal method.
3. To study the physicochemical properties of the synthesized NPs using various analytical techniques.

4. To evaluate and study the ORR activity of the synthesized NPs in alkaline media for long-term stability and durability.
5. To elucidate the role of non-noble transition metals in Pd/C in forming active, highly durable and stable electrocatalysts for ORR in alkaline media.

References

[1] Stambouli, A.B. Fuel cells: The expectations for an environmental-friendly and sustainable source of energy. *Renewable and Sustainable Energy Reviews*, 15(9):4507-4520, 2011.

[2] Singla, M.K., Nijhawan, P. and Oberoi, A.S. Hydrogen fuel and fuel cell technology for cleaner future: a review. *Environmental Science and Pollution Research*, 28(13):15607-15626, 2021.

[3] Staffell, I., Scamman, D., Abad, A.V., Balcombe, P., Dodds, P.E., Ekins, P., Shah, N. and Ward, K.R. The role of hydrogen and fuel cells in the global energy system. *Energy & Environmental Science*, 12(2):463-491, 2019.

[4] Ganiyu, S.O. and Martinez-Huitle, C.A. The use of renewable energies driving electrochemical technologies for environmental applications. *Current Opinion in Electrochemistry*, 22:211-220, 2020.

[5] Hou, H., Lu, W., Liu, B., Hassanein, Z., Mahmood, H. and Khalid, S. Exploring the role of fossil fuels and renewable energy in determining environmental sustainability: Evidence from OECD countries. *Sustainability*, 15(3):2048, 2023.

[6] Masa, J., Andronescu, C. and Schuhmann, W. Electrocatalysis as the nexus for sustainable renewable energy: The gordian knot of activity, stability, and selectivity. *Angewandte Chemie International Edition*, 59(36):15298-15312, 2020.

[7] Li, L., Lin, J., Wu, N., Xie, S., Meng, C., Zheng, Y., Wang, X. and Zhao, Y. Review and outlook on the international renewable energy development. *Energy and Built Environment*, 3(2):139-157, 2022.

[8] PatiL, M.B., Bhagat, S.L., Sapkal, R.S. and Sapkal, V.S. A review on the fuel cells development. *Scientific Reviews & Chemical Communications*, 1(1):25-41, 2011.

[9] Cheng, F. and Chen, J. Metal–air batteries: from oxygen reduction electrochemistry to cathode catalysts. *Chemical Society Reviews*, 41(6):2172-2192, 2012.

[10] Carrette, L., Friedrich, K.A. and Stimming, U. Fuel cells: principles, types, fuels, and applications. *ChemPhysChem*, 1(4):162-193, 2000.

[11] Muthukumar, M., Rengarajan, N., Velliyangiri, B., Omprakas, M.A., Rohit, C.B. and Raja, U.K. The development of fuel cell electric vehicles–A review. *Materials Today: Proceedings*, 45:1181-1187, 2021.

[12] Fan, L., Tu, Z. and Chan, S.H. Recent development of hydrogen and fuel cell technologies: A review. *Energy Reports*, 7:8421-8446, 2021.

[13] Abdelkareem, M.A., Elsaid, K., Wilberforce, T., Kamil, M., Sayed, E.T. and Olabi, A. Environmental aspects of fuel cells: A review. *Science of the Total Environment*, 752:141803, 2021.

[14] Chen, Z., Higgins, D., Yu, A., Zhang, L. and Zhang, J. A review on non-precious metal electrocatalysts for PEM fuel cells. *Energy & Environmental Science*, 4(9):3167-3192, 2011.

[15] Chetry, R., Goswami, C., Borah, B.J. and Bharali, P. Morphology-and size-selective Pd-based electrocatalyst for fuel cell reactions. In Sudarsanam, P., Yamauchi, Y., Bharali P., editors, Heterogeneous nanocatalysis for energy and environmental sustainability, volume 1, Chap 8, pages 233-257, ISBN: 9781394183517, Wiley, 2022.

[16] Mekhilef, S., Saidur, R. and Safari, A. Comparative study of different fuel cell technologies. *Renewable and Sustainable Energy Reviews*, 16(1):981-989, 2012.

[17] Shao, Z. and Ni, M. Fuel cells: Materials needs and advances. *MRS Bulletin*, 49:451-463, 2024.

[18] Antolini, E. The stability of molten carbonate fuel cell electrodes: A review of recent improvements. *Applied Energy*, 88(12):4274-4293, 2011.

[19] Ebrahimi, M., Kujawski, W., Fatyeyeva, K. and Kujawa, J. A review on ionic liquids-based membranes for middle and high temperature polymer electrolyte membrane fuel cells (PEMCs). *International Journal of Molecular Sciences*, 22(11):5430, 2021.

[20] Fan, J., Chen, M., Zhao, Z., Zhang, Z., Ye, S., Xu, S., Wang, H. and Li, H. Bridging the gap between highly active oxygen reduction reaction catalysts and effective catalyst layers for proton exchange membrane fuel cells. *Nature Energy*, 6(5):475-486, 2021.

[21] Qu, E., Hao, X., Xiao, M., Han, D., Huang, S., Huang, Z., Wang, S. and Meng, Y. Proton exchange membranes for high temperature proton exchange membrane fuel cells: Challenges and perspectives. *Journal of Power Sources*, 533:231386, 2022.

[22] Sundmacher, K., Schultz, T., Zhou, S., Scott, K., Ginkel, M. and Gilles, E.D. Dynamics of the direct methanol fuel cell (DMFC): experiments and model-based analysis. *Chemical Engineering Science*, 56(2):333-341, 2001.

[23] Singh, M., Zappa, D. and Comini, E. Solid oxide fuel cell: Decade of progress, future perspectives and challenges. *International Journal of Hydrogen Energy*, 46(54):27643-27674, 2021.

[24] Hussain, S., Erikson, H., Kongi, N., Sarapuu, A., Solla-Gullón, J., Maia, G., Kannan, A.M., Alonso-Vante, N. and Tammeveski, K. Oxygen reduction reaction on nanostructured Pt-based electrocatalysts: A review. *International Journal of Hydrogen Energy*, 45(56):31775-31797, 2020.

[25] Debe, M.K. Electrocatalyst approaches and challenges for automotive fuel cells. *Nature*, 486(7401):43-51, 2012.

[26] Wang, Q., Guesmi, H., Tingry, S., Cornu, D., Holade, Y. and Minteer, S.D. Unveiling the pitfalls of comparing oxygen reduction reaction kinetic data for Pd-based electrocatalysts without the experimental conditions of the current–potential curves. *ACS Energy Letters*, 7(3):952-957, 2022.

[27] Kocha, S.S., Shinozaki, K., Zack, J.W., Myers, D.J., Kariuki, N.N., Nowicki, T., Stamenkovic, V., Kang, Y., Li, D. and Papageorgopoulos, D. Best practices and testing protocols for benchmarking ORR activities of fuel cell electrocatalysts using rotating disk electrode. *Electrocatalysis*, 8:366-374, 2017.

[28] Xia, W., Mahmood, A., Liang, Z., Zou, R. and Guo, S. Earth-abundant nanomaterials for oxygen reduction. *Angewandte Chemie International Edition*, 55(8):2650-2676, 2016.

[29] Li, D., Batchelor-McAuley, C. and Compton, R.G. Some thoughts about reporting the electrocatalytic performance of nanomaterials. *Applied Materials Today*, 18:100404, 2020.

[30] Dix, S.T., Lu, S. and Linic, S. Critical practices in rigorously assessing the inherent activity of nanoparticle electrocatalysts. *ACS Catalysis*, 10(18):10735-10741, 2020.

[31] Mayrhofer, K.J.J., Strmcnik, D., Blizanac, B.B., Stamenkovic, V., Arenz, M. and Markovic, N.M. Measurement of oxygen reduction activities via the rotating disc electrode method: From Pt model surfaces to carbon-supported high surface area catalysts. *Electrochimica Acta*, 53(7): 3181-3188, 2008.

[32] Liu, M., Xiao, X., Li, Q., Luo, L., Ding, M., Zhang, B., Li, Y., Zou, J. and Jiang, B. Recent progress of electrocatalysts for oxygen reduction in fuel cells. *Journal of Colloid and Interface Science*, 607:791-815, 2022.

[33] Wang, X., Li, Z., Qu, Y., Yuan, T., Wang, W., Wu, Y. and Li, Y. Review of metal catalysts for oxygen reduction reaction: from nanoscale engineering to atomic design. *Chem*, 5(6):1486-1511, 2019.

[34] Shao, M., Chang, Q., Dodelet, J.P. and Chenitz, R. Recent advances in electrocatalysts for oxygen reduction reaction. *Chemical Reviews*, 116(6):3594-3657, 2016.

[35] Ge, X., Sumboja, A., Wuu, D., An, T., Li, B., Goh, F.T., Hor, T.A., Zong, Y. and Liu, Z. Oxygen reduction in alkaline media: From mechanisms to recent advances of catalysts. *ACS Catalysis*, 5(8), 4643-4667, 2015.

[36] Stacy, J., Regmi, Y.N., Leonard, B. and Fan, M. The recent progress and future of oxygen reduction reaction catalysis: A review. *Renewable and Sustainable Energy Reviews*, 69:401-414, 2017.

[37] Zhao, Y., Adiyeri Saseendran, D.P., Huang, C., Triana, C.A., Marks, W.R., Chen, H., Zhao, H. and Patzke, G.R. Oxygen evolution/reduction reaction catalysts: From in situ monitoring and reaction mechanisms to rational design. *Chemical Reviews*, 123(9):6257-6358, 2023.

[38] Chetry, R., Bhuyan, S. P., and Bharali P. Bimetallic nanoparticles & their applications for oxygen reduction reaction (ORR) and urea oxidation reaction (UOR). In Gogoi P. Sarmah J. K., Saikia, P. editors, Bimetals: Formation, Properties and Applications, Chap 3, ISBN: 979-8-89113-496-6, Nova Science Publishers, 2024.

[39] Bhuvanendran, N., Ravichandran, S., Xu, Q., Maiyalagan, T. and Su, H. A quick guide to the assessment of key electrochemical performance indicators for the oxygen reduction reaction: A comprehensive review. *International Journal of Hydrogen Energy*, 47(11):7113-7138, 2022.

[40] Shinozaki, K., Zack, J.W., Richards, R.M., Pivovar, B.S. and Kocha, S.S. Oxygen reduction reaction measurements on platinum electrocatalysts utilizing rotating disk electrode technique: I. Impact of impurities, measurement protocols and applied corrections. *Journal of the Electrochemical Society*, 162(10):F1144, 2015.

[41] Bard, A.J. Faulkner, L.R., White, H.S., Electrochemical methods fundamentals and applications. ISBN:978-0-471-04372-0, 2nd John Wiley & Sons, 2022.

[42] Huang, Z.F., Wang, J., Peng, Y., Jung, C.Y., Fisher, A. and Wang, X. Design of efficient bifunctional oxygen reduction/evolution electrocatalyst: Recent advances and perspectives. *Advanced Energy Materials*, 7(23):1700544, 2017.

[43] Wang, T., Chutia, A., Brett, D.J., Shearing, P.R., He, G., Chai, G. and Parkin, I.P. Palladium alloys used as electrocatalysts for the oxygen reduction reaction. *Energy & Environmental Science*, 14(5):2639-2669, 2021.

[44] Li, C.J., Shan, G.C., Guo, C.X. and Ma, R.G. Design strategies of Pd-based electrocatalysts for efficient oxygen reduction. *Rare Metals*, 42(6):1778-1799, 2023.

[45] Xiong, D., Li, X., Fan, L. and Bai, Z. Three-dimensional heteroatom-doped nanocarbon for metal-free oxygen reduction electrocatalysis: A review. *Catalysts*, 8(8):301, 2018.

[46] Porter, N.S., Wu, H., Quan, Z. and Fang, J. Shape-control and electrocatalytic activity-enhancement of Pt-based bimetallic nanocrystals. *Accounts of Chemical Research*, 46(8):1867-1877, 2013.

[47] Zhou, M., Wang, H.L. and Guo, S. Towards high-efficiency nanoelectrocatalysts for oxygen reduction through engineering advanced carbon nanomaterials. *Chemical Society Reviews*, 45(5):1273-1307, 2016.

[48] Nørskov, J.K., Rossmeisl, J., Logadottir, A., Lindqvist, L.R.K.J., Kitchin, J.R., Bligaard, T. and Jonsson, H. Origin of the overpotential for oxygen reduction at a fuel-cell cathode. *The Journal of Physical Chemistry B*, 108(46):17886-17892, 2004.

[49] Sanij, F.D., Balakrishnan, P., Leung, P., Shah, A., Su, H. and Xu, Q. Advanced Pd-based nanomaterials for electro-catalytic oxygen reduction in fuel cells: A review. *International Journal of Hydrogen Energy*, 46(27):14596-14627, 2021.

[50] Goswami, C., Saikia, H., Tada, K., Tanaka, S., Sudarsanam, P., Bhargava, S.K. and Bharali, P. Bimetallic palladium–nickel nanoparticles anchored on carbon as

high-performance electrocatalysts for oxygen reduction and formic acid oxidation reactions. *ACS Applied Energy Materials*, 3(9):9285-9295, 2020.

[51] Zamora Zeledón, J.A., Stevens, M.B., Gunasooriya, G.K.K., Gallo, A., Landers, A.T., Kreider, M.E., Hahn, C., Nørskov, J.K. and Jaramillo, T.F. Tuning the electronic structure of Ag-Pd alloys to enhance performance for alkaline oxygen reduction. *Nature Communications*, 12(1):620, 2021.

[52] Zhang, Z., Liu, S., Tian, X., Wang, J., Xu, P., Xiao, F. and Wang, S. Facile synthesis of N-doped porous carbon encapsulated bimetallic PdCo as a highly active and durable electrocatalyst for oxygen reduction and ethanol oxidation. *Journal of Materials Chemistry A*, 5(22):10876-10884, 2017.

[53] Wang, Y., Zhu, Z., Xu, K., Guo, W., Yu, T., He, M., Wei, W. and Yang, T. Palladium nanobelts with expanded lattice spacing for electrochemical oxygen reduction in alkaline media. *ACS Applied Nano Materials*, 4(2):2118-2125, 2021.

[54] Zhang, L.Y., Guo, C.X., Cao, H., Wang, S., Ouyang, Y., Xu, B., Guo, P. and Li, C.M. Highly wrinkled palladium nanosheets as advanced electrocatalysts for the oxygen reduction reaction in acidic medium. *Chemical Engineering Journal*, 431:133237, 2022.

[55] Liu, M., Lyu, Z., Zhang, Y., Chen, R., Xie, M. and Xia, Y. Twin-directed deposition of Pt on Pd icosahedral nanocrystals for catalysts with enhanced activity and durability toward oxygen reduction. *Nano Letters*, 21(5):2248-2254, 2021.

[56] Gebre, S.H. and Sendeku, M.G. Trimetallic nanostructures and their applications in electrocatalytic energy conversions. *Journal of Energy Chemistry*, 65:329-351, 2022.

[57] Crawley, J.W., Gow, I.E., Lawes, N., Kowalec, I., Kabalan, L., Catlow, C.R.A., Logsdail, A.J., Taylor, S.H., Dummer, N.F. and Hutchings, G.J. Heterogeneous trimetallic nanoparticles as catalysts. *Chemical Reviews*, 122(6):6795-6849, 2022.

[58] Rodrigues, T.S., da Silva, A.G. and Camargo, P.H. Nanocatalysis by noble metal nanoparticles: Controlled synthesis for the optimization and understanding of activities. *Journal of Materials Chemistry A*, 7(11):5857-5874, 2019.

[59] Wang, H., Yin, S., Li, Y., Yu, H., Li, C., Deng, K., Xu, Y., Li, X., Xue, H., Wang, L. One-Step fabrication of tri-metallic PdCuAu nanothorn assemblies as an

efficient catalyst for oxygen reduction reaction. *Journal of Materials Chemistry A*, 6(8):3642-3648, 2018.

[60] Zhen, C., Lyu, Z., Liu, K., Chen, X., Sun, Y., Liao, X., Xie, S. Ultrasmall PdPtCo trimetallic nanorings with enriched low-coordinated edge sites and optimized compositions for effective oxygen reduction electrocatalysis. *CrystEngComm*, 23(29):5033-5038, 2021.

[61] Wang, H., Yin, S., Xu, Y., Li, X., Alshehri, A.A., Yamauchi, Y., Xue, H., Kaneti, Y.V. Wang, L. Direct fabrication of tri-metallic PtPdCu tripods with branched exteriors for the oxygen reduction reaction. *Journal of Materials Chemistry A*, 6(18):8662-8668, 2018.

[62] Kong, F., Liu, S., Li, J., Du, L., Banis, M.N., Zhang, L., Chen, G., Doyle-Davis, K., Liang, J., Wang, S., Zhao, F. Trimetallic Pt–Pd–Ni octahedral nanocages with subnanometer thick-wall towards high oxygen reduction reaction. *Nano Energy*, 64:103890, 2019.

[63] Zhu, Y., Wang, S., Luo, Q., Huang, H., Tang, S., Du, Y. Facile synthesis of structurally ordered low-Pt-loading Pd–Pt–Fe nanoalloys with enhanced electrocatalytic performance for oxygen reduction reaction. *Journal of Alloys and Compounds*, 855:157322, 2021.

[64] Wang, H., Ren, H., Liu, S., Yin, S., Jiao, S., Xu, Y., Li, X., Wang, Z. and Wang, L. Three-dimensional PdAuRu nanospines assemblies for oxygen reduction electrocatalysis. *Chemical Engineering Journal*, 438:135539, 2022.

[65] Wu, X., Liu, X., He, Y., Lei, L., Hao, S. and Zhang, X. A ternary PdNiMo alloy as a bifunctional nanocatalyst for the oxygen reduction reaction and hydrogen evolution reaction. *Inorganic Chemistry Frontiers*, 9(24):6574-6583, 2022.

[66] Wang, H., Li, L., Sheng, S., Wang, C., Qu, T., Hou, D., Wang, D. and Sheng, M. Synthesis of low-cost Co-Sn-Pd/rGO catalysts via ultrasonic irradiation and their electrocatalytic activities toward oxygen reduction reaction. *The Canadian Journal of Chemical Engineering*, 100:S160-S171, 2022.

[67] Li, C., Yuan, Q., Ni, B., He, T., Zhang, S., Long, Y., Gu, L. and Wang, X. Dendritic defect-rich palladium–copper–cobalt nanoalloys as robust multifunctional non-platinum electrocatalysts for fuel cells. *Nature Communications*, 9(1):3702, 2018.

[68] Sun, L., Liao, B., Ren, X., Li, Y., Zhang, P., Deng, L. and Gao, Y. Ternary PdNi-based nanocrystals supported on nitrogen-doped reduced graphene oxide as highly active electrocatalysts for the oxygen reduction reaction. *Electrochimica Acta*, 235:543-552, 2017.

[69] Xue, Y., Sun, S., Wang, Q., Dong, Z. and Liu, Z. Transition metal oxide-based oxygen reduction reaction electrocatalysts for energy conversion systems with aqueous electrolytes. *Journal of Materials Chemistry A*, 6(23):10595-10626, 2018.

[70] Wang, Y., Li, J. and Wei, Z. Transition-metal-oxide-based catalysts for the oxygen reduction reaction. *Journal of Materials Chemistry A*, 6(18):8194-8209, 2018.

[71] Sun, M., Liu, H., Liu, Y., Qu, J., and Li, J. Graphene-based transition metal oxide nanocomposites for the oxygen reduction reaction. *Nanoscale*, 7(4):1250–1269, 2015.

[72] Vellacheri, R., Unni, S.M., Nahire, S., Kharul, U.K. and Kurungot, S. Pt–MoO_x-carbon nanotube redox couple based electrocatalyst as a potential partner with polybenzimidazole membrane for high temperature polymer electrolyte membrane fuel cell applications. *Electrochimica Acta*, 55(8):2878-2887, 2010.

[73] Choi, C.H., Park, S.H. and Woo, S.I. Oxygen reduction activity of Pd–Mn_3O_4 nanoparticles and performance enhancement by voltammetrically accelerated degradation. *Physical Chemistry Chemical Physics*, 14(19):6842-6848, 2012.

[74] Zhang, Z., Wang, X., Cui, Z., Liu, C., Lu, T. and Xing, W. Pd nanoparticles supported on WO_3/C hybrid material as catalyst for oxygen reduction reaction. *Journal of Power Sources*, 185(2):941-945, 2008.

[75] Dhali, S., Pandey, S., Dandapat, A., Sahoo, T., Sahu, P.S., Saha, B. and Sahoo, N.G. Pd-Fe_2O_3 decorated nitrogen-doped reduced graphene oxide/CNT nanohybrids electrocatalyst for proton exchange membrane fuel cell. *Diamond and Related Materials*, 126:109115, 2022.

[76] Sharma, S. and Pollet, B.G. Support materials for PEMFC and DMFC electrocatalysts—A review. *Journal of Power Sources*, 208:96-119, 2012.

[77] Erikson, H., Sarapuu, A., Solla-Gullón, J. and Tammeveski, K. Recent progress in oxygen reduction electrocatalysis on Pd-based catalysts. *Journal of Electroanalytical Chemistry*, 780:327-336, 2016.

[78] Wang, Y.J., Wilkinson, D.P. and Zhang, J. Noncarbon support materials for polymer electrolyte membrane fuel cell electrocatalysts. *Chemical reviews*, 111(12):7625-7651, 2011.

[79] Zhou, X., Qiao, J., Yang, L. and Zhang, J. A review of graphene-based nanostructural materials for both catalyst supports and metal-free catalysts in PEM fuel cell oxygen reduction reactions. *Advanced Energy Materials*, 4(8):1301523, 2014.

[80] Xiang, Q., Yu, J. and Jaroniec, M. Graphene-based semiconductor photocatalysts. *Chemical Society Reviews*, 41(2):782-796, 2012.

[81] Zhu, C. and Dong, S. Recent progress in graphene-based nanomaterials as advanced electrocatalysts towards oxygen reduction reaction. *Nanoscale*, 5(5):1753-1767, 2013.

[82] Novoselov, K.S., Fal'ko V. I., Colombo, L., Gellert, P.R., Schwab, M.G. and Kim and K. A roadmap for graphene. *Nature*, 490:192-200, 2012.